NASA/TP–2013-217803

Faster Heavy Ion Transport for HZETRN

Tony C. Slaba
Langley Research Center, Hampton, Virginia

February 2013

NASA STI Program . . . in Profile

Since its founding, NASA has been dedicated to the advancement of aeronautics and space science. The NASA scientific and technical information (STI) program plays a key part in helping NASA maintain this important role.

The NASA STI program operates under the auspices of the Agency Chief Information Officer. It collects, organizes, provides for archiving, and disseminates NASA's STI. The NASA STI program provides access to the NASA Aeronautics and Space Database and its public interface, the NASA Technical Report Server, thus providing one of the largest collections of aeronautical and space science STI in the world. Results are published in both non-NASA channels and by NASA in the NASA STI Report Series, which includes the following report types:

- TECHNICAL PUBLICATION. Reports of completed research or a major significant phase of research that present the results of NASA Programs and include extensive data or theoretical analysis. Includes compilations of significant scientific and technical data and information deemed to be of continuing reference value. NASA counterpart of peer-reviewed formal professional papers, but having less stringent limitations on manuscript length and extent of graphic presentations.

- TECHNICAL MEMORANDUM. Scientific and technical findings that are preliminary or of specialized interest, e.g., quick release reports, working papers, and bibliographies that contain minimal annotation. Does not contain extensive analysis.

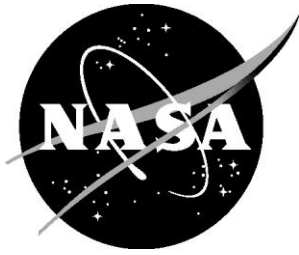- CONTRACTOR REPORT. Scientific and technical findings by NASA-sponsored contractors and grantees.

- CONFERENCE PUBLICATION. Collected papers from scientific and technical conferences, symposia, seminars, or other meetings sponsored or co-sponsored by NASA.

- SPECIAL PUBLICATION. Scientific, technical, or historical information from NASA programs, projects, and missions, often concerned with subjects having substantial public interest.

- TECHNICAL TRANSLATION. English-language translations of foreign scientific and technical material pertinent to NASA's mission.

Specialized services also include organizing and publishing research results, distributing specialized research announcements and feeds, providing information desk and personal search support, and enabling data exchange services.

For more information about the NASA STI program, see the following:

- Access the NASA STI program home page at *http://www.sti.nasa.gov*

- E-mail your question to help@sti.nasa.gov

- Fax your question to the NASA STI Information Desk at 443-757-5803

- Phone the NASA STI Information Desk at 443-757-5802

- Write to:
  STI Information Desk
  NASA Center for AeroSpace Information
  7115 Standard Drive
  Hanover, MD 21076-1320

Faster Heavy Ion Transport for HZETRN

Tony C. Slaba
Langley Research Center, Hampton, Virginia

February 2013

Contents

Figures

Tables

Abstract

The deterministic particle transport code HZETRN was developed to enable fast and accurate space radiation transport through materials. As more complex transport solutions are implemented for neutrons, light ions (Z ≤ 2), mesons, and leptons, it is important to maintain overall computational efficiency. In this work, the heavy ion (Z > 2) transport algorithm in HZETRN is reviewed, and a simple modification is shown to provide an approximate 5x decrease in execution time for galactic cosmic ray transport. Convergence tests and other comparisons are carried out to verify that numerical accuracy is maintained in the new algorithm.

1. Introduction

The deterministic particle transport code, HZETRN (High charge (Z) and Energy TRaNsport) [Wilson et al. 1991; Slaba et al. 2010a, 2010b], is a fast and accurate computational tool for transporting space radiation through shielding materials and human tissue. Recent updates to the code have provided significant reductions in run time [Slaba et al. 2010a], and further work reduced overall discretization error to less than 4% for shielding materials and thicknesses commonly found in space applications [Slaba et al. 2012a]. This increased efficiency has enabled new calculations that would have otherwise been computationally prohibitive. First, a ray-by-ray transport methodology has been developed wherein transport is explicitly performed along each ray direction in a shielding thickness distribution, and no constraint is placed on the number or ordering of materials along a ray [Slaba et al. 2011a]. Second, the transport of pions, muons, electrons, positrons, and photons has been added into HZETRN at a moderate computational cost [Norman et al. 2012a, 2012b; Slaba et al. 2012b]. Third, calculations may be performed through detailed vehicle geometry on a minute-by-minute basis along a trajectory. This type of analysis has been useful in providing more rigorous validation comparisons and uncertainty estimates [Slaba et al. 2011b, 2012b].

Further developments that lead to more efficient numerical methods or algorithms are beneficial and may also enable new analyses to be completed. In this work, the heavy ion (Z > 2) transport algorithm in HZETRN is reviewed, and a simple modification is made that allows interpolation to be avoided in the ion collision source term. It is shown that the modification provides an approximate 5x decrease in execution time without sacrificing numerical accuracy.

2. Heavy Ion Transport Formalism

In this section, the heavy ion transport formalism in HZETRN is reviewed. The Boltzmann transport equation with the continuous slowing down and straight ahead approximations is given as [Wilson et al. 1991]

$$\overline{B}[\phi_j(x,E)] = \sum_k \int_E^\infty \sigma_{jk}(E,E')\phi_k(x,E')\,dE',\tag{1}$$

with the linear differential operator

$$\overline{B}[\phi_j(x,E)] \equiv \left[\frac{\partial}{\partial x} - \frac{1}{A_j}\frac{\partial}{\partial E}S_j(E) + \sigma_j(E)\right]\phi_j(x,E),\tag{2}$$

and boundary condition

$$\phi_j(0,E) = f_j(E).\tag{3}$$

1

In equations (1) - (3), $\phi_j(x,E)$ is the flux of type j particles at depth x with kinetic energy E, A_j is the atomic mass number of a type j particle, $S_j(E)$ is the stopping power of a type j ion with kinetic energy E, $\sigma_j(E)$ is the total macroscopic cross section for a type j particle with kinetic energy E, and $\sigma_{jk}(E,E')$ is the differential macroscopic production cross section for interactions in which a type k particle with kinetic energy E' produces a type j particle with kinetic energy E. The summation limits in equation (1) are taken over all projectiles that might produce a given fragment. The boundary condition spectrum, $f_j(E)$, is considered to be a known function over a broad energy spectrum.

The ion stopping powers, $S_j(E)$, in equation (2) may be approximated in terms of the proton stopping power, $S(E)$, as [Bethe et al. 1930]

$$\frac{1}{A_j}S_j(E) \approx \nu_j S(E), \tag{4}$$

where the scaling parameter is expressed in terms of the ion mass and charge (A_j, Z_j) according to $\nu_j = Z_j^2 / A_j$. The transport equation may now be written as

$$B[\phi_j(x,E)] = \sum_k \int_E^\infty \sigma_{jk}(E,E')\phi_k(x,E')\,dE', \tag{5}$$

with the modified linear differential operator

$$B[\phi_j(x,E)] \equiv \left[\frac{\partial}{\partial x} - \nu_j \frac{\partial}{\partial E}S(E) + \sigma_j(E)\right]\phi_j(x,E). \tag{6}$$

Approximating the ion stopping powers with the scaled proton stopping power allows simplified numerical algorithms, as has been discussed elsewhere [Wilson et al. 2006].

For heavy ions, it is noted that projectile fragments have an energy and direction very near that of the projectile, while target fragments are produced nearly isotropically with low energy and travel only a short distance before being absorbed [Wilson et al. 2006]. The approximate decoupling of target and projectile fragments is discussed in detail by Wilson et al. [1995] and suggests that target fragments can be neglected in the heavy ion transport procedure (their contribution to dose is approximately accounted for after the transport procedure). The equal velocity assumption for heavy ions can be expressed in the production cross section as [Shinn et al. 1992]

$$\sigma_{jk}(E,E') = \sigma_{jk}(E')\delta(E-E'), \tag{7}$$

where $\sigma_{jk}(E)$ is the partial fragmentation cross section for interactions in which a type k particle with kinetic energy E produces a type j particle. In this case, equation (5) becomes

$$B[\phi_j(x,E)] = \sum_k \sigma_{jk}(E)\phi_k(x,E). \tag{8}$$

The absence of target fragments in the heavy ion transport procedure allows one to take the summation in equation (5) over all projectiles with mass greater than that of the fragment. If all the transported particles are ordered according to mass, then equation (5) can be succinctly written as

$$B[\phi_j(x,E)] = \sum_{k>j} \sigma_{jk}(E)\phi_k(x,E), \tag{9}$$

which is the transport equation found in Wilson et al. [2006] and will be referred to as the heavy ion transport equation. The upper summation limit in equation (9) can vary, but it is common to use no fewer than 59 ions [Cucinotta et al. 2006].

For light particles (n, p, ^{2}H, ^{2}H, ^{3}He, ^{4}He), both projectile and target fragments are included in the transport procedure. The broad energy distribution in collision events also indicates that the equal velocity assumption in equation (7) cannot be used. In this case, no simplifications to equation (5) are available, and the summation is taken over all light particles. It should be noted that for solar particle events with a negligible heavy ion component, only the solution to the light particle transport equation is required. For galactic cosmic ray (GCR) environments, there are both heavy ion and light ion components, and solutions to the light particle and heavy ion transport equations must be evaluated simultaneously. The light particle transport solutions and coupling to heavy ion transport has been discussed in detail elsewhere [Slaba et al. 2010a] and will not be repeated here.

3. Heavy Ion Marching Equation

In this section, the mathematical formalism that allows equation (9) to be inverted and expressed as an explicit marching procedure is reviewed. The following derivation was taken from Wilson et al. [1977, 1986, 1991, 1995, 2006] and Shinn et al. [1992]. The scaled heavy ion flux is defined as

$$\psi_j(x,r) \equiv \nu_j S(E)\phi_j(x,E) \,, \tag{10}$$

where r is the proton range defined in terms of the stopping power according to the equation

$$r \equiv \int_0^E \frac{dE'}{S(E')} \,. \tag{11}$$

Equation (9) may be written in terms of the scaled flux and proton range as

$$\left[\frac{\partial}{\partial x} - \nu_j \frac{\partial}{\partial r} + \sigma_j(r) \right] \psi_j(x,r) = \sum_{k>j} \frac{\nu_j}{\nu_k} \sigma_{jk}(r)\psi_k(x,r) \,, \tag{12}$$

where the quantities, $\sigma_j(E)$ and $\sigma_{jk}(E)$ have been replaced with $\sigma_j(r)$ and $\sigma_{jk}(r)$ since, for a given r, equation (11) may be inverted to find E. Equation (12) may be inverted using the method of characteristics to obtain the Volterra integral equation

$$\psi_j(x,r) = e^{-\beta_j(r,x)}\psi_j(0, r + \nu_j x)$$
$$+ \sum_{k>j} \frac{\nu_j}{\nu_k} \int_0^x e^{-\beta_j(r,x')} \sigma_{jk}\left(r + \nu_j x'\right)\psi_k\left(x - x', r + \nu_j x'\right) dx' \,, \tag{13}$$

with the exponential term

$$\beta_j(r,x) = \int_0^x \sigma_j(r + \nu_j t)dt \,. \tag{14}$$

The complete details of how equation (9) is transformed into equation (12) as well as the inversion of equation (12) have been given by Slaba et al. [2010c]. Equation (13) may be written as a marching procedure in terms of a step-size, h, as

$$\psi_j(x+h,r) = e^{-\beta_j(r,h)}\psi_j(x,r+\nu_j h)$$
$$+\sum_{k>j}\frac{\nu_j}{\nu_k}\int_0^h e^{-\beta_j(r,x')}\sigma_{jk}\left(r+\nu_j x'\right)\psi_k\left(x+h-x',r+\nu_j x'\right)dx' . \tag{15}$$

The integrand in equation (15) is approximated by considering the solution to the homogeneous form of equation (12). The homogeneous equation neglects secondary particle production through nuclear interactions and accounts only for the slowing down of particles due to atomic interactions and the loss of particles due to nuclear absorption. If the step-size is taken to be sufficiently small such that

$$h \ll \frac{1}{\sigma_j(r)}, \tag{16}$$

(i.e. much less than the nuclear mean free path), then the local truncation error will be negligible as the particles will not have travelled far enough to participate in a nuclear collision [Wilson et al. 1991]. The homogeneous solution is given by the equation [Wilson et al. 2006]

$$\psi_j(x+h,r) = e^{-\beta_j(r,h)}\psi_j(x,r+\nu_j h), \tag{17}$$

which may be equivalently written as

$$\psi_k(x+h-x',r+\nu_j x') = e^{-\beta_k(r+\nu_j x',h-x')}\psi_k(x,r+\nu_j x'+\nu_k(h-x')), \tag{18}$$

and substituted into equation (15) to obtain

$$\psi_j(x+h,r) = e^{-\beta_j(r,h)}\psi_j(x,r+\nu_j h)$$
$$+\sum_{k>j}\frac{\nu_j}{\nu_k}\int_0^h e^{-\beta_j(r,x')-\beta_k(r+\nu_j x',h-x')}\sigma_{jk}\left(r+\nu_j x'\right)\psi_k(x,r+\nu_j x'+\nu_k(h-x'))dx' . \tag{19}$$

The fragmentation cross section and particle flux appearing in the integrand of equation (19) are approximated as

$$\sigma_{jk}\left(r+\nu_j x'\right) \approx \sigma_{jk}\left(r+\nu_j h/2\right), \tag{20}$$

$$\psi_k(x,r+\nu_j x'+\nu_k(h-x')) \approx \psi_k(x,r+(\nu_j+\nu_k)h/2). \tag{21}$$

Equation (20) is accurate since heavy ion fragmentation cross sections vary slowly as a function of energy (range), and most collisions occur at energies for which the ion range is large compared to typical step-sizes. Equation (21) is accurate since the scaled heavy ion fluxes are nearly constant at low range values. At higher range values, the step-size is comparatively small, and the step-size perturbation has a small affect. These statements are supported in Figure 1, showing representative fragmentation cross sections and scaled ion fluxes as a function of proton range (bottom axis) and kinetic energy (top axis).
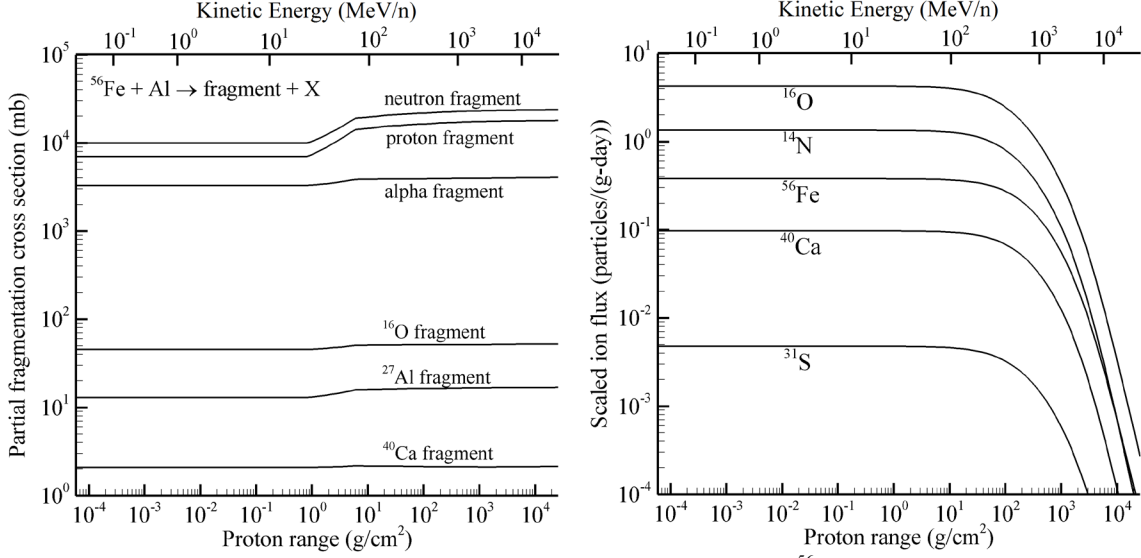
Figure 1. The left pane shows the partial fragmentation cross section for ^{56}Fe + Al as a function of proton range and kinetic energy. The right pane shows the scaled ion fluxes at 20 g/cm^2 in aluminum exposed to solar minimum GCR conditions given by the Badhwar-O'Neill 2010 model [O'Neill 2010] with a solar modulation parameter of 475 MV.

Upon substitution of equations (20) and (21), the heavy ion transport equation becomes

$$\psi_j(x + h, r) = e^{-\beta_j(r,h)}\psi_j(x, r + \nu_j h)$$
$$+ \sum_{k>j} \frac{\nu_j}{\nu_k} \sigma_{jk}\left(r + \nu_j h / 2\right)\psi_k(x, r + (\nu_j + \nu_k)h / 2)\int_0^h e^{-\beta_j(r,x') - \beta_k(r + \nu_j x', h - x')}\, dx'. \tag{22}$$

The remaining integral is evaluated by expanding the exponential terms in the integrand of equation (22). The complete details of the expansion and integral evaluation have been given by Slaba et al. [2010c]. The integral is approximately evaluated as

$$\int_0^h e^{-\beta_j(r,x') - \beta_k(r + \nu_j x', h - x')}\, dx' \approx \frac{e^{-\sigma_j(r + \nu_j h/2)h} - e^{-\sigma_k(r + (\nu_j + \nu_k)h/2)h}}{\sigma_k(r + (\nu_j + \nu_k)h / 2) - \sigma_j(r + \nu_j h / 2)} \tag{23}$$
$$\equiv C_{jk}(r).$$

The final marching procedure is now given by the equation

$$\psi_j(x + h, r) = e^{-\beta_j(r,h)}\psi_j(x, r + \nu_j h)$$
$$+ \sum_{k>j} \frac{\nu_j}{\nu_k} \sigma_{jk}\left(r + \nu_j h / 2\right)\psi_k(x, r + (\nu_j + \nu_k)h / 2)C_{jk}(r), \tag{24}$$

This is the heavy ion marching equation given by Wilson et al. [2006]. The heavy ion fluxes are evaluated on a pre-defined energy grid that is converted to proton range values. There are typically 100 grid points spaced logarithmically from 0.01 MeV/n to 50 GeV/n. In order to obtain the ion flux at a grid point, r_i, interpolation is needed to evaluate the terms $\psi_j(x, r + \nu_j h)$ and $\psi_k(x, r + (\nu_j + \nu_k)h / 2)$. The interpolation method that has been typically used in HZETRN is log-log cubic Lagrange [Wilson et al. 1995]. In this method, the logarithm of both the dependent and independent variables is evaluated. A cubic Lagrange interpolation scheme is applied, and the resulting value is exponentiated.

5

4. New Numerical Method

In this section, the original numerical implementation of the heavy ion marching equation is modified to provide a more efficient algorithm. As stated in the previous section, interpolation is required to evaluate the ion fluxes at values not on the prescribed energy/range grid. By examining the summation term in equation (24), it can be determined that the number of interpolations per marching step scales linearly with the number of energy grid points and quadratically with the number of isotopes. For typical calculations, this number is on the order of 10^3 interpolations per step. For a given range value, r_i, an alternative strategy to evaluate equation (24) is to use the nearest-neighbor approximation

$$\psi_k(x, r_i + (\nu_j + \nu_k)h \,/\, 2) \approx \psi_k(x, r_i^*), \tag{25}$$

where r_i^* is the nearest grid point value to $r_i + (\nu_j + \nu_k)h \,/\, 2$. For each r_i, the heavy ion marching equation becomes

$$
\begin{aligned}
\psi_j(x + h, r_i) &= e^{-\beta_j(r_i, h)} \psi_j(x, r_i + \nu_j h) \\
&+ \sum_{k > j} \frac{\nu_j}{\nu_k} \sigma_{jk}\left(r_i + \nu_j h \,/\, 2\right) \psi_k(x, r_i^*) C_{jk}(r_i).
\end{aligned} \tag{26}
$$

In this equation, no interpolation is needed to evaluate the ion flux within the production summation. Consequently, the only interpolation required is for $\psi_j(x, r_i + \nu_j h)$, and the total number of interpolations per step is now directly proportional the number of energy grid points. In order to take advantage of the nearest neighbor approach, the mapping from each r_i to the nearest neighbor of $r_i + (\nu_j + \nu_k)h \,/\, 2$ is evaluated once and used repeatedly throughout code execution. As in the previous section, equation (25) is accurate at low range values since the scaled ion fluxes are nearly constant in this region. At higher range values, the step-size perturbation has a small effect. Further, the number of grid points typically used for heavy ion transport provides sufficient fidelity so that the nearest-neighbor range value is not far from the actual perturbed value.

It should be noted that at the first step from the front boundary, secondary ion fluxes are changing rapidly, and the previous heavy ion solution is more accurate than equation (26). Similar behavior is observed near material interfaces, but the impact is less noticeable than at the front boundary. In the updated heavy ion algorithm, a hybrid approach has been adopted. For the first step into any material, including material interfaces, the original heavy ion marching equation (24) is evaluated. All other steps use the simplified form in equation (26). Log-log cubic Lagrange interpolation is still used to evaluate the term $\psi_j(x, r_i + \nu_j h)$.

5. Flux Comparison

In this section, a flux-based comparison between the original and new heavy ion transport algorithms is given. In this comparison, both algorithms were used to transport a solar minimum GCR environment through a 100 g/cm^2 aluminum slab and a 100 g/cm^2 water slab, and fluxes were saved at various depths in both slabs. The solar minimum GCR environment was calculated with the Badhwar-O'Neill 2010 GCR model [O'Neill 2010] using a solar modulation parameter of 475 MV. The relative difference between the results computed with both algorithms is computed as

$$\overline{R}_j(E_i, x_k) = \frac{\phi_j^{(N)}(E_i, x_k) - \phi_j^{(O)}(E_i, x_k)}{\phi_j^{(O)}(E_i, x_k)}, \tag{27}$$

where $\phi_j^{(O)}(E_i, x_k)$ and $\phi_j^{(N)}(E_i, x_k)$ are the fluxes for each ion, j, at each energy, E_i, and depth, x_k, computed with the original (O) and new (N) algorithms, respectively. It was found that the absolute value of the relative difference between the old and new algorithms never exceeded 5% over all energies, ions, and depths. In order to summarize these results, the following quantities were computed as a function of energy,

$$R_{\min}(E_i) = \min_{j,k} \bar{R}_j(E_i, x_k) \tag{28}$$

$$R_{\max}(E_i) = \max_{j,k} \bar{R}_j(E_i, x_k) \tag{29}$$

$$R_{\text{avg}}(E_i) = \frac{1}{N_j N_x} \sum_{k=1}^{N_x} \sum_{j=1}^{N_j} \bar{R}_j(E_i, x_k) \tag{30}$$

$$R_{\text{sd}}(E_i) = \sqrt{\frac{1}{N_j N_x} \sum_{k=1}^{N_x} \sum_{j=1}^{N_j} \left[\bar{R}_j(E_i, x_k) - R_{\text{avg}}(E_i) \right]^2} \tag{31}$$

Equations (28) - (31) have also been computed as a function of particle type and depth. The results are shown in Figures 2 - 4. The symbol in each figure is the average of the relative differences, $R_{\text{avg}}(E_i)$. The outer-most error bars represent the minimum and maximum relative differences defined in equations (28) and (29). The inner-most error bars represent the standard deviation of relative differences defined in equation (31). The standard deviation error bars indicate where most of the relative differences occur, while the minimum/maximum error bars indicate the extreme values of relative differences. The absolute value of all relative differences is clearly within 5%, and most relative differences are within 2%. This indicates that the simpler nearest-neighbor interpolation approach gives results that are very similar to the more complicated and computationally expensive log-log cubic Lagrange method. It should also be noted that the relative differences shown in Figures 2 – 4 translate into relative differences for dose equivalent that are bounded by 0.3%. It will be shown later, that the increased speed provided by the nearest neighbor approach justifies this negligible loss in accuracy.
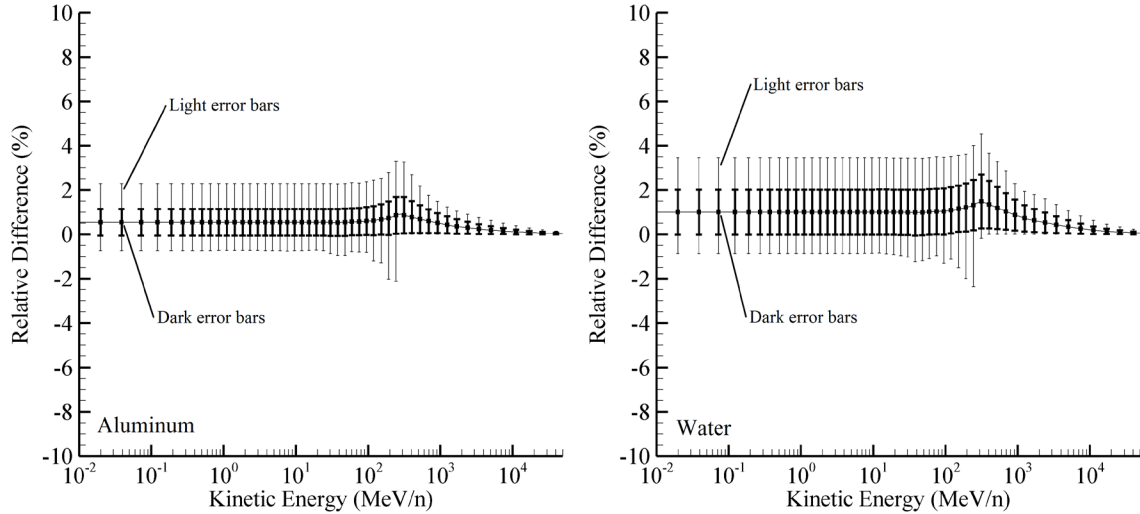

Figure 2. Relative difference between fluxes computed by the original and modified heavy ion transport algorithm as a function of kinetic energy in aluminum and water exposed to solar minimum GCR conditions. Light and dark error bars represent extreme and standard deviation of relative differences, respectively.
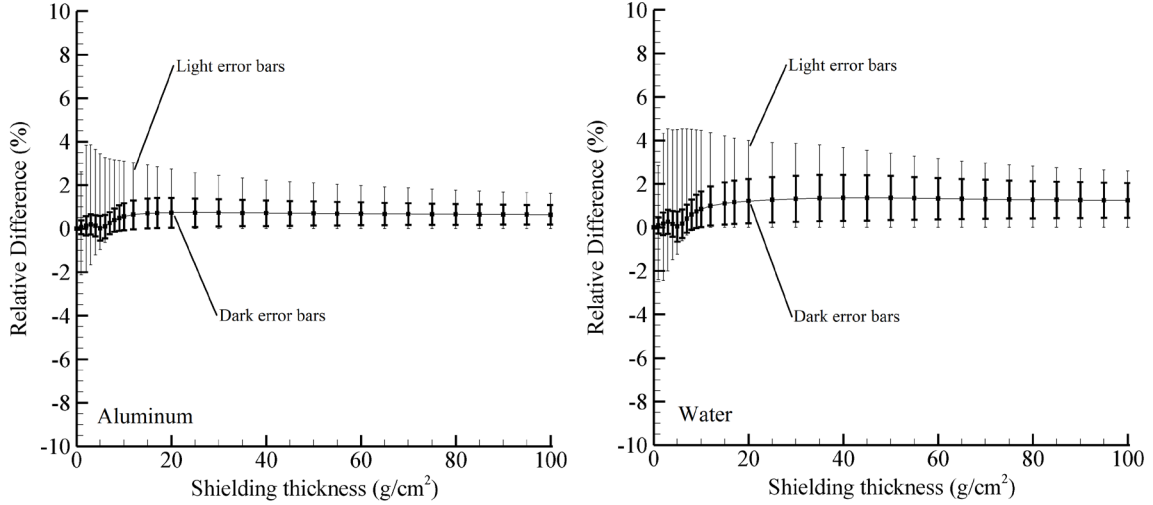
Figure 3. Relative difference between fluxes computed by the original and modified heavy ion transport algorithm as a function of shielding thickness in aluminum and water exposed to solar minimum GCR conditions. Light and dark error bars represent extreme and standard deviation of relative differences, respectively.
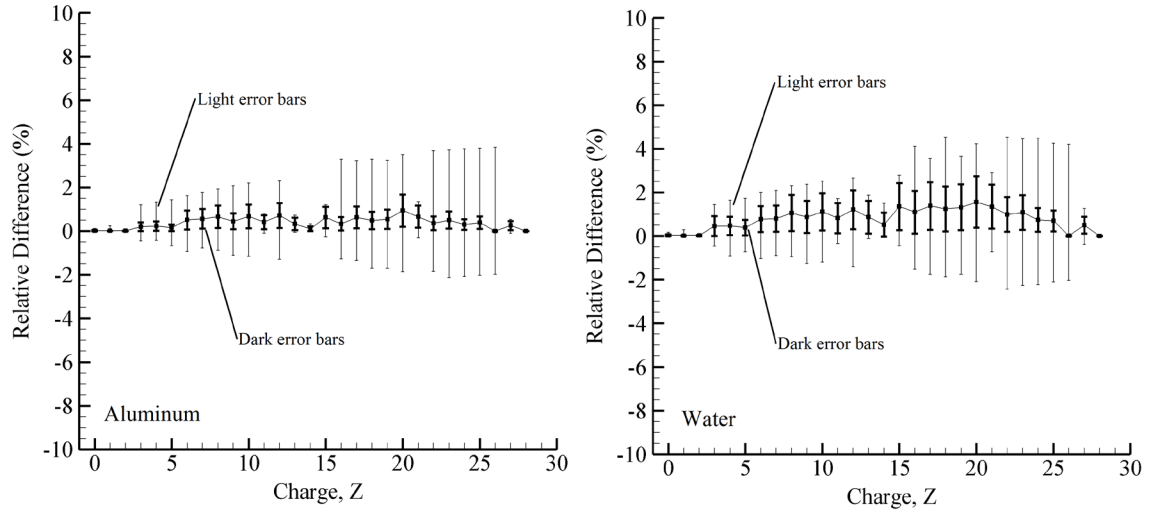

Figure 4. Relative difference between fluxes computed by the original and modified heavy ion transport algorithm as a function of charge in aluminum and water exposed to solar minimum GCR conditions. Light and dark error bars represent extreme and standard deviation of relative differences, respectively.

6. Convergence Test

A computational algorithm is said to converge if the numerical solutions reach an asymptotic limit as the discretization parameters approach zero. HZETRN has two discretization parameters: the step size, h, and the number of energy grid points, N. In order to show convergence and quantify discretization error, discretization parameters are refined several times and the differences between the various solutions are compared. This process is referred to as a convergence test.

In this section, convergence tests are applied to the original and modified heavy ion transport algorithms to show convergence and quantify overall discretization error. Five different energy grid sizes are considered ranging from $N = 100$ to $N = 502$, along with eleven different step-sizes ranging from $h =$

8

0.5 g/cm^2 to $h = 2^{-11}$ g/cm^2. These discretization parameters are used in both the original and modified heavy ion transport algorithms to transport a solar minimum GCR environment through 100 g/cm^2 of aluminum and water. The solar minimum GCR environment was calculated with the Badhwar-O'Neill 2010 GCR model [O'Neill 2010] using a solar modulation parameter of 475 MV. The same light particle transport algorithm was coupled to both the original and new heavy ion transport algorithm. Dose equivalent is computed at a number of depths in the slab and is used as the quantity of interest for the error analysis.

Dose equivalent as a function of depth in aluminum and water exposed to the solar minimum GCR environment is given in Figure 5 for both algorithms and all of the discretization parameters. The data in Figure 5 show that both algorithms with the various discretization parameters give very similar results over the thicknesses considered. The spread in dose equivalent values at 100 g/cm^2 in aluminum and water is 1.2% and 1.4%, respectively. This variation includes both the differences associated with the original and new heavy ion transport algorithm as well as the inherent discretization errors.
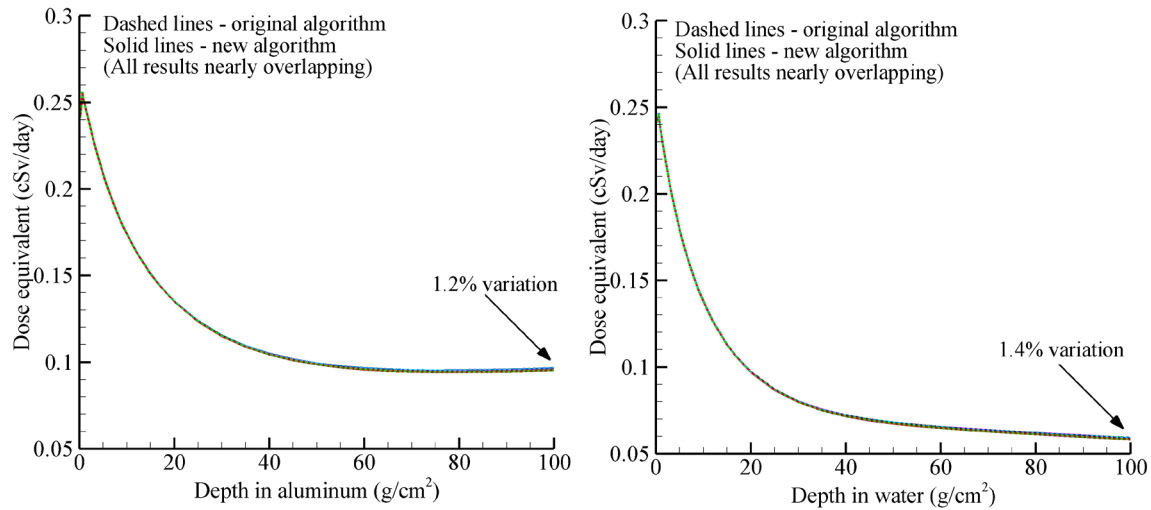
Figure 5. Dose equivalent versus depth in aluminum (left pane) and water (right pane) exposed to solar minimum GCR conditions computed with the original and modified heavy ion transport algorithms and all discretization parameters.
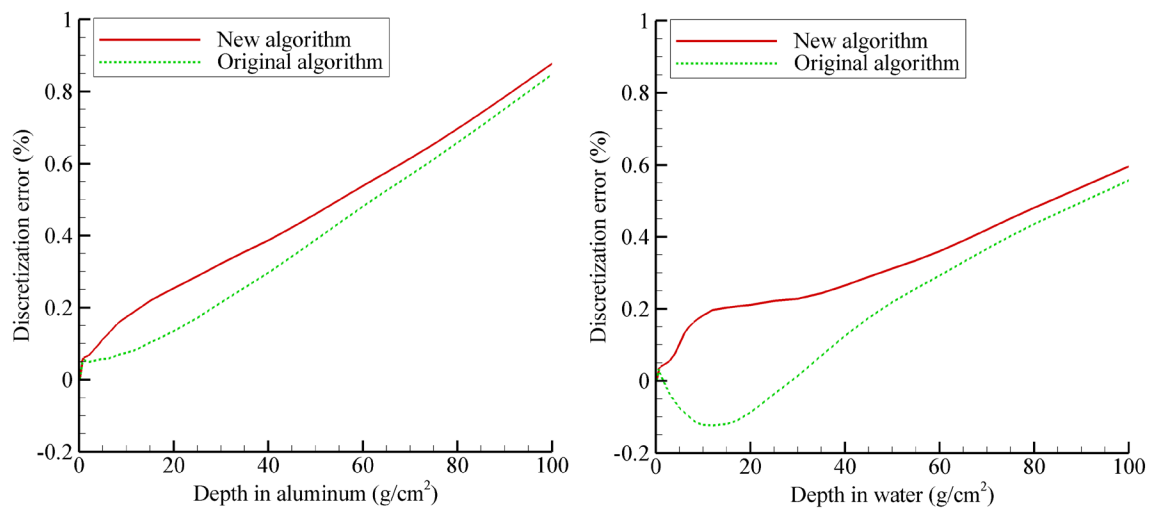
Figure 6. Total discretization error for dose equivalent as a function of depth in aluminum (left pane) and water (right pane) exposed to a solar minimum GCR environment.

9

The total discretization error associated with the original and modified heavy ion transport algorithms for aluminum and water targets exposed to the solar minimum GCR environment is shown in Figure 6. For each algorithm, the discretization error is obtained by computing the relative percent difference between the converged results obtained with fine discretization parameters ($h = 2^{-11}$ g/cm^2 and $N = 502$) and the solution obtained with typical discretization parameters ($h = 0.5$ g/cm^2 and $N = 100$). A negative discretization error indicates that the results obtained with the typical discretization parameters underestimate the converged result. It is clear that the modified heavy ion transport algorithm results in a negligible increase in discretization error in both aluminum and water targets as thick as 100 g/cm^2. It will be shown in the next section that this minor loss of accuracy is justified by the significant reduction in code run time.

7. Run-time Comparisons

The original and modified heavy ion transport algorithms are used to transport the same solar minimum GCR boundary condition through three different shielding configurations typically used with HZETRN. The solar minimum GCR environment was calculated with the Badhwar-O'Neill 2010 GCR model [O'Neill 2010] using a solar modulation parameter of 475 MV. These run-time tests were performed on a Linux computer with 8 quad-core AMD Opteron 8378 processors and 256 GB of RAM. Each test was run 25 times with the original and new algorithms, and the reported run-times are the average of the 25 separate executions. Results are given in Table 1. The column labeled "1 layer" corresponds to a shielding configuration made of a single layer of aluminum. This type of calculation might be done to analyze the radiation protection properties of a slab of some material or to generate a simplified interpolation database for vehicle analysis. The column labeled "2 layer" corresponds to a shielding configuration made of an aluminum shield followed by a tissue target. Fluxes are stored on a two-dimensional grid of points covering every combination of first and second layer thicknesses. This simulation is typically used to model a shielding structure (aluminum) surrounding a human phantom (tissue). The column labeled "3 layer" corresponds to an aluminum shield followed by a polyethylene shield and a tissue target. This simulation is typically used to model a shielding structure (aluminum) with a secondary shield (polyethylene) surrounding a human phantom (tissue). In all three cases, the maximum thickness of any layer is 100 g/cm^2, and each layer has 11 spatial grid points spaced nearly logarithmically at which fluxes are saved and printed to a file. Results are given in Table 1.

Table 1. Run-time (seconds) comparisons between original and new heavy ion transport algorithms.

	1 layer	2 layer	3 layer
Original	9.2	96.1	1042.3
New	2.9	20.1	212.4
Factor	3.2	4.8	4.9

The overhead computational cost of reading in cross section databases and writing out flux files is the same in both codes and is included in the total run-time. Consequently, the ratio between the original and new run times is not constant. Two additional 1-layer tests were run, but the slab thickness was increased to 1000 g/cm^2 and 5000 g/cm^2, and the fluxes were only printed out at the front and back boundaries of the slab to minimize the run-time dedicated to file writing. These tests help minimize the impact of reading and writing data on total run-time and more clearly show the increased speed associated with the new algorithm. It was found that the new code was 5.5x and 5.8x faster than the old code in the 1000 g/cm^2 and 5000 g/cm^2 slabs, respectively.

8. Conclusions

In this work, a modification to the heavy ion transport algorithm in HZETRN was shown to be approximately 5x faster than the original algorithm, and convergence tests showed that the loss in numerical accuracy was negligible (< 1%). This increase in overall code run time for GCR calculations will

be beneficial for future analysis including risk assessment, ray-by-ray calculations, and geometries with large shielding thicknesses such as the International Space Station and martian atmosphere.

9. References

Bethe, Von H., Zur Theorie des Durchgangs schneller Korpuskularstraheln durch Materie. Annals of Physics, 5 Folge, Bd. 5, pp. 325-400 (1930).

Cucinotta, F.A., Wilson, J.W., Saganti, P., Hu, X., Kim, M.Y., Cleghorn, T., Zeitlin, C., Tripathi, R.K., Isotopic Dependence of GCR Fluence behind Shielding. Radiation Measurements, Volume 41, pp. 1235-1249 (2006).

Norman, R.B., Blattnig, S.R., De Angelis, G., Badavi, F.F., Norbury, J.W., Deterministic Pion and Muon Transport in Earth's Atmosphere. Advances in Space Research, Volume 50, pp. 146-155 (2012a).

Norman, R.B., Slaba, T.C., Blattnig, S.R., An Extension of HZETRN for Cosmic Ray Initiated Electromagnetic Cascades. Advances in Space Research, accepted for publication (2012b).

O'Neill, P.M., Badhwar-O'Neill Galactic Cosmic Ray Flux Model – Revised. IEEE Transactions on Nuclear Science, Volume 57, pp. 3148 – 3153 (2010).

Shinn, J.L., John, S., Tripathi, R.K., Wilson, J.W., Townsend, L.W., Norbury, J.W., A Fully Energy-Dependent HZETRN (A Galactic Cosmic-Ray Transport Code). NASA Technical Paper 3243 (1992).

Slaba, T.C., Blattnig, S.R., Badavi, F.F., Faster and more Accurate Transport Procedures for HZETRN. Journal of Computational Physics, Volume 229, pp. 9397-9417 (2010a).

Slaba, T.C., Blattnig, S.R., Aghara, S.K., Townsend, L.W., Handler, T., Gabriel, T.A., Pinsky, L.S., Reddell, B., Coupled Neutron Transport for HZETRN. Radiation Measurements, Volume 45 pp. 173-182 (2010b).

Slaba, T.C., Blattnig, S.R., Badavi, F.F., Faster and more Accurate Transport Procedures for HZETRN. NASA Technical Paper 2010 – 216213 (2010c).

Slaba, T.C., Blattnig, S.R., Clowdsley, M.S., Variations in Lunar Neutron Dose Estimates. Radiation Research, Volume 176, pp. 827-841 (2011a).

Slaba, T.C., Blattnig, S.R., Badavi, F.F., Stoffle, N.N., Rutledge, R.D., Lee, K.T., Zapp, E.N., Dachev, Ts. P., Tomov, B.T., Statistical Validation of HZETRN as a Function of Vertical Cutoff Rigidity using ISS Measurements. Advances in Space Research, Volume 47, pp. 600-610 (2011b).

Slaba, T.C., Blattnig, S.R., Tweed, J., Reduced Discretization Error in HZETRN. Journal of Computational Physics, Volume 234, pp. 217-229 (2012a).

Slaba, T.C., Blattnig, S.R., Reddell, B., Bahadori, A., Norman, R.B., Badavi, F.F., Pion and Electromagnetic Contribution to Dose: Comparisons of HZETRN to Monte Carlo Results and ISS Data. Advances in Space Research, submitted (2012b).

Wilson, J.W., Analysis of the Theory of Heavy Ion Transport. NASA Technical Note D-8381 (1977).

Wilson, J.W. and Badavi, F.F., Methods of Galactic Heavy Ion Transport. Radiation Research, Volume 108, pp. 231-237 (1986).

Wilson, J.W., Townsend, L.W., Schimmerling, W., Khandelwal, G.S., Khan, F., Nealy, J.E., Cucinotta, F.A., Simonsen, L.C., Shinn, J.L., Norbury, J.W., Transport Methods and Interactions for Space Radiations. NASA Reference Publication 1257 (1991).

Wilson, J.W., Badavi, F.F., Cucinotta, F.A., Shinn, J.L., Badhwar, G.D, Silberberg, R., Tsao, C.H., Townsend, L.W., Tripathi, R.K., HZETRN: Description of a Free-Space Ion and Nucleon Transport and Shielding Computer Program. NASA Technical Paper 3495 (1995).

Wilson, J.W., Tripathi, R.K., Badavi, F.F., Cucinotta, F.A., Standardized Radiation Shield Design Method: 2005 HZETRN. SAE ICES 2006-18 (2006).

REPORT DOCUMENTATION PAGE		*Form Approved* *OMB No. 0704-0188*

1. REPORT DATE *(DD-MM-YYYY)* 01- 02 - 2013	2. REPORT TYPE Technical Publication	3. DATES COVERED *(From - To)*

4. TITLE AND SUBTITLE

Faster Heavy Ion Transport for HZETRN

5a. CONTRACT NUMBER

5b. GRANT NUMBER

5c. PROGRAM ELEMENT NUMBER

6. AUTHOR(S)

Slaba, Tony C.

5d. PROJECT NUMBER

5e. TASK NUMBER

5f. WORK UNIT NUMBER
651549.02.07.10

7. PERFORMING ORGANIZATION NAME(S) AND ADDRESS(ES)
NASA Langley Research Center
Hampton, VA 23681-2199

8. PERFORMING ORGANIZATION REPORT NUMBER

L-20222

9. SPONSORING/MONITORING AGENCY NAME(S) AND ADDRESS(ES)
National Aeronautics and Space Administration
Washington, DC 20546-0001

10. SPONSOR/MONITOR'S ACRONYM(S)

NASA

11. SPONSOR/MONITOR'S REPORT NUMBER(S)
NASA/TP-2013-217803

12. DISTRIBUTION/AVAILABILITY STATEMENT
Unclassified - Unlimited
Subject Category 93
Availability: NASA CASI (443) 757-5802

13. SUPPLEMENTARY NOTES

14. ABSTRACT

The deterministic particle transport code HZETRN was developed to enable fast and accurate space radiation transport through materials. As more complex transport solutions are implemented for neutrons, light ions ($Z < 2$), mesons, and leptons, it is important to maintain overall computational efficiency. In this work, the heavy ion ($Z > 2$) transport algorithm in HZETRN is reviewed, and a simple modification is shown to provide an approximate 5x decrease in execution time for galactic cosmic ray transport. Convergence tests and other comparisons are carried out to verify that numerical accuracy is maintained in the new algorithm.

15. SUBJECT TERMS

HZETRN; Heavy ions; Radiation transport; Space radiation

16. SECURITY CLASSIFICATION OF:			17. LIMITATION OF ABSTRACT	18. NUMBER OF PAGES	19a. NAME OF RESPONSIBLE PERSON STI Help Desk (email: help@sti.nasa.gov)
a. REPORT	b. ABSTRACT	c. THIS PAGE			
U	U	U	UU	20	19b. TELEPHONE NUMBER *(Include area code)* (443) 757-5802

Standard Form 298 (Rev. 8-98)
Prescribed by ANSI Std. Z39.18